Development of Effective Taylor-Quinney Coefficient Table of *MAT_224 for Aluminum 2024-T351

Chung-Kyu Park[1], Kelly Carney[1], Paul Du Bois[1], and Cing-Dao Kan[1]

[1] Center for Collision Safety and Analysis, George Mason University, Fairfax, VA, USA

Abstract
In this research work, the effective Taylor-Quinney Coefficient (TQC) table of ***MAT_224** for Aluminum 2024-T351 alloy was developed to replace the current constant TQC. The methodology to create the effective TQC table was developed by using a two-step approach. In Step 1, the thermal-structural analyses of tensile tests were conducted to verify the referenced TQC values and generate the additional temperature-strain curves at additional rates which were not covered by the physical tensile tests. In Step 2, the structural-only analyses of tensile tests were conducted to calibrate the effective TQC values at all the rates for the effective TQC table and validate the calibrated effective TQC table.

1 Introduction

A team consisting of George Mason University, Ohio State University, George Washington University, the National Aeronautics and Space Administration - Glenn Research Center, and the Federal Aviation Administration - Aircraft Catastrophic Failure Prevention Program collaborated to develop a new constitutive material model in LS-DYNA for metallic materials. The research was directed toward improving the numerical modeling of turbine engine blade-out containment tests required for the certification of aircraft engines [1]. In this effort, the LS-DYNA constitutive material model ***MAT_TABULATED_JOHNSON_COOK**, or simply ***MAT_224**, was developed [2]. ***MAT_224** is a general elasto-thermo-visco-plastic material model that utilizes a tabulated approach to incorporate arbitrary stress versus strain curves to define material plasticity, including arbitrary strain rate and temperature dependency. Adiabatic heating due to plastic work can cause temperatures to increase and the material to soften. Rupture is modeled by an element erosion criterion using plastic strain, which can be defined as a function of the state of stress, strain rate, temperature, and element size.

As an extension of these efforts, ***MAT_224** input parameters of Aluminum 2024-T351 alloy (Al2024) have been developed and released publicly. The Al2024 dataset (Version 2.2) of ***MAT_224** was developed [3-6] and validated intensively with several series of ballistic impact simulations: (1) ballistic impact simulations of a sphere projectile to square Al2024 plates with various thicknesses [3,7], (2) ballistic impact simulations of a cylinder projectile onto circular Al2024 plates with various thicknesses [3,8], (3) ballistic impact simulations of 1/8-inch thick Al2024 plates with rectangular projectiles, having varying oblique incidence and attitude angles [8,9], and (4) ballistic impact simulations on large flat Al2024 panels with a blade-shaped Titanium 6Al-4V alloy projectile designed to represent key aspects of a real turbine engine fan-blade release event [10]. Overall, the ballistic impact simulations showed good correlations to the lab tests for a broad range of test conditions.

The thermal softening of metallic materials is the result of a stiffness reduction caused by temperature rise induced by heating from plastic deformation of the material. The thermal softening is dependent on the temperature field governed by heat generation and dissipation over the period of plastic deformation that occurs in the material. Although in general, the heat dissipation includes the combined effects of conduction, convection, and radiation, here, conduction is the dominant mechanism. When the plastic deformation rate of the material is high enough to neglect the heat conduction in the material, thermal softening occurs in an adiabatic condition. Conversely, if the plastic deformation happens in a quasi-static condition, it becomes an isothermal process, the material's temperature remains nearly constant, and there is little or no thermal softening. Originally, the ***MAT_224** constitutive model was developed for the analysis of high-speed impact problems occurring on a short timescale, e.g., determining whether an engine containment case is breached by impact of a fan blade fragment. In such high-speed impact problems, it is naturally assumed that a metallic material is deformed under an adiabatic condition. To that end, the ***MAT_224** constitutive model implemented a function to calculate the temperature increase induced by plastic work, and its utilization ignored all heat dissipation.

In ***MAT_224** the temperature rise is estimated using the Taylor-Quinney Coefficient (TQC), or symbolically Beta (β), which describes the percentage of plastic work converted into heat energy. The physical TQC constant of Al2024 obtained from references [11] was adopted in the development of the ***MAT_224** dataset of Al2024. The ***MAT_224** material model of Al2024, with the constant physical TQC, produced good correlated simulations both to high-rate mechanical property tests, and ballistic impact tests. However, the constant physical TQC in the current Al2024 material model of ***MAT_224** could be problematic for the impact analysis of a full engine structure where the strain rate ranges from quasi-static to extremely high rates near the impact. The constant physical TQC could also be problematic for longer duration analysis where the strain rate decreases after the initial impact's extremely high rates. Depending on the rates of material deformation, the thermal softening of material transits from an isothermal process at a quasi-static rate to an adiabatic process at a high rate, which is distinguished by how much heat is conducted in the thermal softening process. Thus, the constant physical TQC could not represent the material thermal softening process in low and intermediate-rate deformation properly without considering heat conduction. So, effective TQCs that consider heat conduction at different rates are required to accurately simulate dynamic processes which involve plastic deformation over a broad range of strain rates.

Material tensile tests of Al2024 were conducted with full-field measurement systems to obtain effective TQC values at various strain rates [12]. Measurement- derived effective TQC values of Al2024 were calculated based on the temperature increase measured at the local failure area of the specimens. The effective TQC values were calculated at the various strain rates of the physical tensile tests. The effective TQC values measured from the temperature and strain field evolution observed in the experiments include the combined effects of heat generation from plastic deformation determined by the physical TQC, and the dissipation by heat conduction. The measured effective TQC can then be defined as a function (table) of the effective TQC values with respect to strain rates. However, this measured effective TQC table cannot be used as a direct input to ***MAT_224** because of fundamental differences in temperature gradients. This difference is due to the absence of the heat conduction term in the ***MAT_224** constitutive model. So, the measured effective TQC table needs to be calibrated by the numerical analysis to develop the calibrated effective TQC table for ***MAT_224**. The calibrated TQC values at low and intermediate strain rates describe temperature rise at each rate associated with both heat generation and conduction.

In this research, the method to calibrate the effective TQC values at different rates was developed through two-step numerical analyses, and the calibrated effective TQC table of Al2024 was obtained and validated. Its extension report including the calibrated effective TQC tables of Titanium 6Al-4V and Inconel 718 Alloys will be published [13].

2 Material tensile tests

Material tensile tests of Al2024 at six different strain rates at room temperature were conducted by the Ohio State University [12]. In these tests, the full-field strain and temperature were measured simultaneously to obtain temperature increase versus strain history and measure the effective TQCs at each rate.

Fig.1(a) shows the curves of measured temperature change versus strain at the local failure point of the specimen at different strain rates. There was negligible temperature change at the quasi-static rate (10-4/sec) in Al2024, which means that the thermal softening was in the isothermal condition. When the rate became higher, like over 500/sec in Al2024, the temperature increased linearly along with strain. In other words, the thermal softening was in the adiabatic condition. It is observed that, at the rate of 0.1/sec in Al2024, the temperature is increasing with decreasing slope due to heat conduction.

Fig.1(b) shows the curves of TQC versus plastic strain at various strain rates in Al2024. The TQC values were measured and averaged over the local failure area of the specimen. In the quasi-static rate (10-4/sec), the TQC is zero because of no temperature change as shown in Fig.1(a). When the rate in the test is higher and the plastic strain gets larger, the TQC value converges to the physical TQC value of Al2024. In the low rates, the TQC values become lower than the physical TQC value due to heat conduction, which is called the effective TQC value. The measured effective TQC values at each rate were obtained by averaging the TQC curves in Fig.1(b). The measured effective TQC table of Al2024 from the tensile tests is summarized in Table 1.

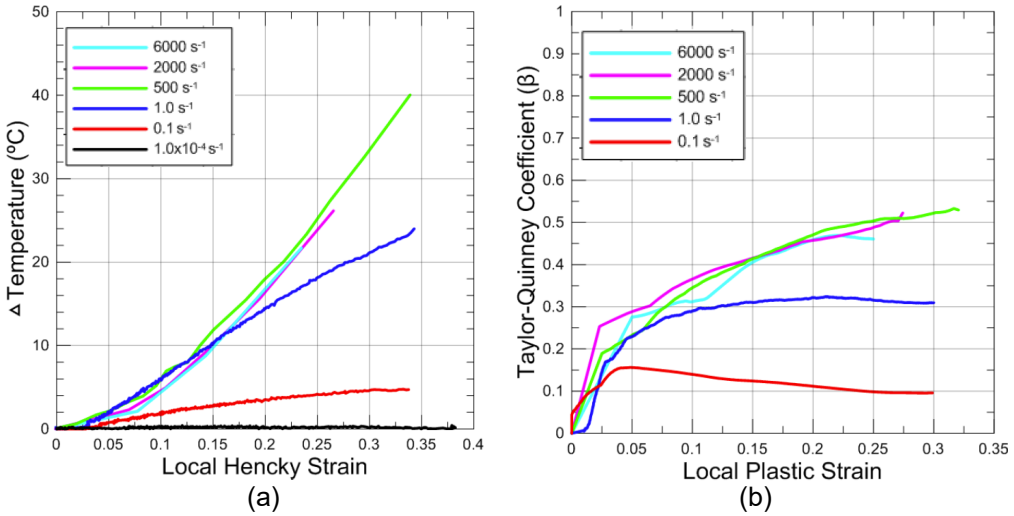

Fig.1: (a) Temperature change vs. strain at the local failure points of the specimen at various rates [12], and (b) TQC vs. plastic strain at the local failure areas of the specimen at various rates [12].

Nominal strain rate (s^{-1})	**SR1**	**SR2**	**SR3**	**SR4**	**SR5**	**SR6**
	0.001	0.1	1.0	500	2,000	6,000
Measured effective TQCs of Al2024	0.0	0.114	0.331	0.533	0.526	0.485

Table 1: Measured effective TQCs at various rates.

3 Thermal softening in `*MAT_224`

In general, the thermal softening of metallic materials is the result of a stiffness reduction caused by heating, and the associated temperature rise induced by plastic deformation of the material. Basically, thermal softening is dependent on heat generation and conduction over the period of plastic deformation that happens in the material, which is governed by the heat equation. The general heat equation is expressed as

$$\frac{\partial T(\mathbf{x},t)}{\partial t} = \frac{1}{\rho c_p}\left\{\nabla \cdot \left(k \cdot \nabla\left(T(\mathbf{x},t)\right)\right) + \dot{q}\right\} \tag{1}$$

where ρ is the density, c_p is the heat capacity, k is the heat conductivity, T is the temperature, and $\dot{q}$ is the rate of the internal heat sources per unit volume. The internal heat sources of solid bodies can be described as heat generation by plastic work and defined as

$$\dot{q} = \beta \sigma_y \dot{\varepsilon}_p \tag{2}$$

where β is the TQC, σ_y is the flow stress, and $\dot{\varepsilon}_p$ is the rate of the plastic strain. The TQC describes the percentage of plastic work converted into heat energy. So, Equation (1) means that the temperature change in the material over time results from heat conduction to and from neighbors surrounding material over time, which is the first term of the right side of Equation (1); and the heat generation induced by plastic deformation, which is the second term of the right side of Equation (1).

Originally, the **`*MAT_224`** constitutive material model was developed for the analysis of high-velocity impact problems, where the thermal softening occurs in an adiabatic condition. So, in **`*MAT_224`**, the temperature change is set so that only heat generation as a result of plastic work is calculated and heat conduction is ignored, which is implemented by

$$\Delta T = \frac{1}{\rho c_p}\int \dot{q}\, dt = \frac{1}{\rho c_p}\int \beta\, \sigma_y \dot{\varepsilon}_p dt \tag{3}$$

Initially, the TQC was defined as a constant in ***MAT_224** and later the TQC was updated to be defined as a function of strain rate, temperature, plastic strain, and the state of stress.

The ***MAT_224** input dataset of Al2024 has been developed starting with the constant physical TQC which is 0.4 from [11]. With a constant physical TQC, the temperature change of a material is dependent only on the plastic work, which is a function of plastic strain, and independent of the strain rate. As a result, the current ***MAT_224** datasets of Al2024 do not represent the thermal softening of materials deforming at low and intermediate strain rates. To overcome this limitation, the TQC value can be adjusted according to the strain rates, which becomes the effective TQC table.

The test-measured effective TQC tables of Al2024 from the tensile tests were shown in Table 1. However, these values cannot be directly used as ***MAT_224** input for two reasons. The first reason is that the data points in the measured effective TQC table obtained from tests are too sparse and deviated to define a smooth TQC vs. rate curve. The other, more fundamental reason is that because of no heat conduction, the temperature versus strain curve from low rate ***MAT_224** simulations is increasing linearly, or with increasing slope. However, in the actual low-rate experiments, due to heat conduction, the temperature versus strain curve has a decreasing slope with increasing temperature. Therefore, the effective TQC values at low rates need to be calibrated for ***MAT_224** input, which is the calibrated effective TQC table.

4 Methodology

The thermal softening of a material can be analyzed by a thermal-structural coupled analysis method in which the structural solver calculates material deformation, and the thermal solver obtains temperature change by heat generation and conduction. Coupled thermal-structural analysis is known to have the capability to make accurate deformation and temperature predictions in metallic materials, achieving good agreement with material tests.

On the other hand, structural-only analysis reduces runtime significantly, but does not include heat conduction. In a structural-only simulation, the ***MAT_224** constitutive material model contains the feature to calculate temperature increases induced by plastic deformation, which allows the thermal softening analysis. However, because ***MAT_224** does not have an independent heat conduction feature, the results between the thermal-structural coupled analysis and structural-only analysis are different at low and intermediate rates. So, the effective TQC values of ***MAT_224** need to be calibrated to match structural-only analysis results with thermal-structural coupled analysis results.

In this study, a method to create the calibrated effective TQC table for ***MAT_224** input was developed as a two-step approach. In the first step, the thermal-structural coupled solver is used to verify the physical TQC values of the materials by comparing numerical results with test results, and to create temperature curves at additional intermediate rates. In the second step, the structural-only solver is used to calibrate the effective TQC values at all rates and to validate the calibrated effective TQC table.

4.1 Step 1: Thermal-structural coupled analysis

In the first step, the thermal-structural coupled solver is used in tensile test simulations to generate the temperature vs. strain curves at additional strain rates that were not covered by the physical tensile tests.

First, the material model of ***MAT_224** that was developed using the structural-only solver need to be verified, confirming that they generate acceptable results in the thermal-structural coupled analysis. Especially, the referenced physical TQC values need to be verified to obtain accurate temperature results. It should be noted that in the LS-DYNA thermal-structural coupled solver, the physical TQC is defined by the FWORK parameter on the ***CONTROL_THERMAL_SOLVER** keyword input. The BETA parameter on the ***MAT_224** keyword input is ignored when using the thermal-structural coupled solver.

All of the physical tensile test series, at all the different rates, are simulated by the thermal-structural coupled solver. The outputs of simulations, such as force-displacement, temperature-strain, and rate-strain curves, are compared with test results to check the accuracy of simulations. Through iterative simulations, the physical TQC is adjusted to bring the simulation results closest to the test outputs.

Second, the additional simulations at extra rates are conducted with the adjusted physical TQC to obtain the additional temperature-strain curves, which provide additional points to the effective TQC table. The additional effective TQC values at extra rates make an effective TQC vs. rate curve smooth over the range of strain rates from isothermal to adiabatic.

4.2 Step 2: Structural-only analysis

In the second step, the structural-only solver is used to develop the effective TQC vs. strain rate table by calibrating the effective TQC values at each rate.

First, tensile test simulations at all rates were conducted by the structural-only solver to obtain their temperature-strain curves. In the structural-only analysis, the adjusted physical TQC in the first step was initially applied to the BETA parameter in ***MAT_224**. The adjusted physical TQC would work for the high-rate simulations but would not for lower rates due to the absence of heat conduction in the structural-only analysis. So, the BETA parameter needs to be calibrated to make temperature-strain curves obtained from the first and second steps comparable to each other.

Fig.2 shows the temperature-strain curves at the SR2 rate obtained from the first and second steps. The temperature-strain curve from the first step shows that the temperature increase slope is decreasing due to heat conduction, but the temperature-strain curves from the second step show nearly linear curves with different slopes depending on the BETA parameter values. These temperature-strain curves have a linear slope because of the absence of heat conduction in the structural-only analysis. So, it is difficult to compare the two curves directly because of the different trends. Instead, the areas under the curves up to a strain of 0.3 can be compared.

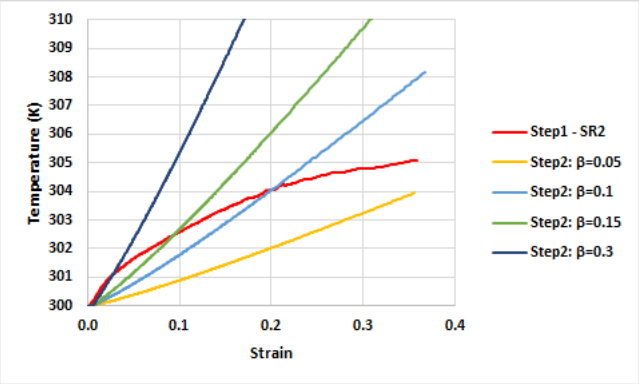

Fig.2: Temperature vs strain curves of Al2024 at the SR2 rate obtained from the first and second steps.

In order to calibrate the effective TQCs at each rate, the BETA parameter in ***MAT_224** can be adjusted through iterative simulations to make two temperature-strain curves from the first and second steps comparable. Alternatively, an approximate method was developed to find the calibrated effective TQCs at each rate by utilizing the linearity of temperature-strain curves in the structural-only analysis. The areas under the temperature-strain curves with different BETA parameter values were also linearly proportional to the BETA parameter values, and so the slope of the area-BETA curve could be obtained. Because the goal was that the areas of the temperature-strain curves from the first and second steps should be the same, the calibrated effective TQC could be estimated by dividing the area of the temperature-strain curve from the first step by the slope of the area-BETA curve from the second step. The calibrated effective TQC table was then developed by gathering the calibrated effective TQCs at all rates. The calibrated effective TQC table could then be validated by comparing its results with physical test results.

5 Finite element model and simulation

The Finite Element (FE) model of the tensile test coupon specimen was developed as shown in Fig.3. The smallest solid element size is about 0.152 mm. The ***MAT_224** material models of Al2024 was used. The ***MAT_THERMAL_ISOTROPIC** was used for the thermal-structural coupled analysis. The initial temperature for all simulations was set to 300 degrees Kelvin because the physical tests were conducted

at room temperature. In the tensile simulations, the strain was obtained by comparing displacements from two nodes, matching the test Digital Image Correlation (DIC) virtual extensometer length shown in Fig.3. The temperature was measured at the center of the specimen where the material failure was initiated. The strain rate curves were obtained by differentiating the strain curves and taking their moving averages to remove noise.

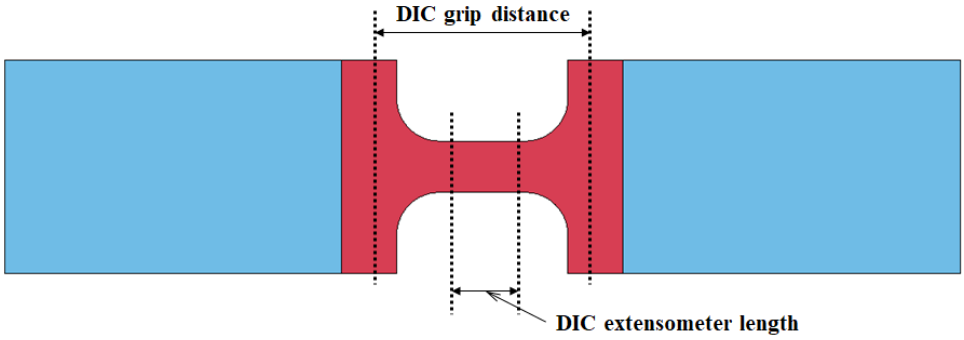

Fig.3: FE model of the coupon specimen of the tensile test.

The physical tensile tests were conducted at six different strain rates, ranging from quasi-static to high rates, as shown in Table 1. In order to simulate them efficiently, the LS-DYNA implicit structural solver was used for quasi-static to low rates, and the LS-DYNA explicit structural solver was used for mid to high rates. In the implicit analysis, a convergence study was conducted to check simulation accuracy.

In the physical mid to high-rate tensile tests, grip slippage often occurs and displacements measured away from the specimen are then inaccurate. The uncertain condition in these specimens makes developing accurate material models problematic. So, in the tests, the DIC camera frame was set up to capture the displacements of both grip locations. Then, the grip displacement history was measured from the DIC image and applied in the simulations as a loading condition, directly at the grip locations, as shown in Fig.3.

6 Effective TQC table creation

The effective TQC table for **`*MAT_224`** material models of Al2024 was created and validated. Simulation results using these tables are summarized in this section. It should be noted that those previously existing metallic material models of *MAT_224 were developed when less test data was available, including no thermal data, and so the referenced physical TQC values were not verified at that time. Therefore, it was not expected that all simulation outputs would agree well with the physical test data.

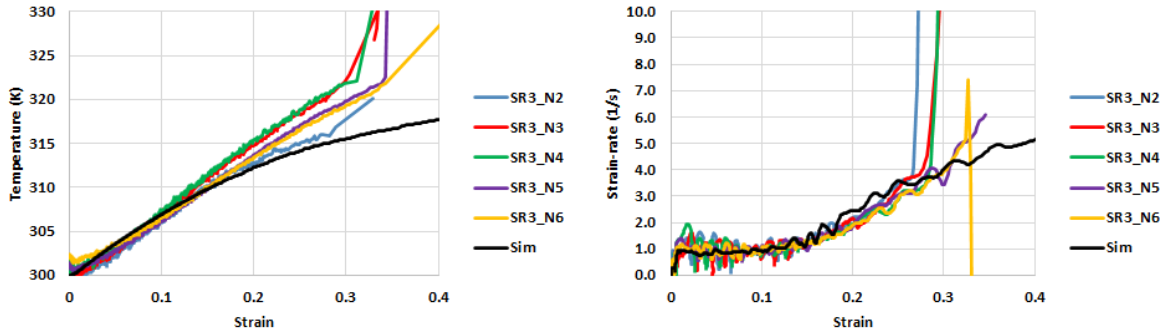

(a) (b)

Fig.4: Comparison between tests and thermal-structural coupled simulations for Al2024 at the SR3 rate; (a) temperature vs. strain, and (b) strain-rate vs. strain.

The repeated thermal-structural coupled analyses in Step 1 determined that the adjusted physical TQC value of Al2024 is 0.5, which is higher than the 0.4 of the referenced physical TQC value. The SR3 and SR5 results of Al2024 tensile simulations at six test rates by the thermal-structural coupled analysis,

using a physical TQC value of 0.5, are shown in Fig.4 and Fig.5. Comparisons with the physical test results include temperature-strain curves and rate-strain curves.

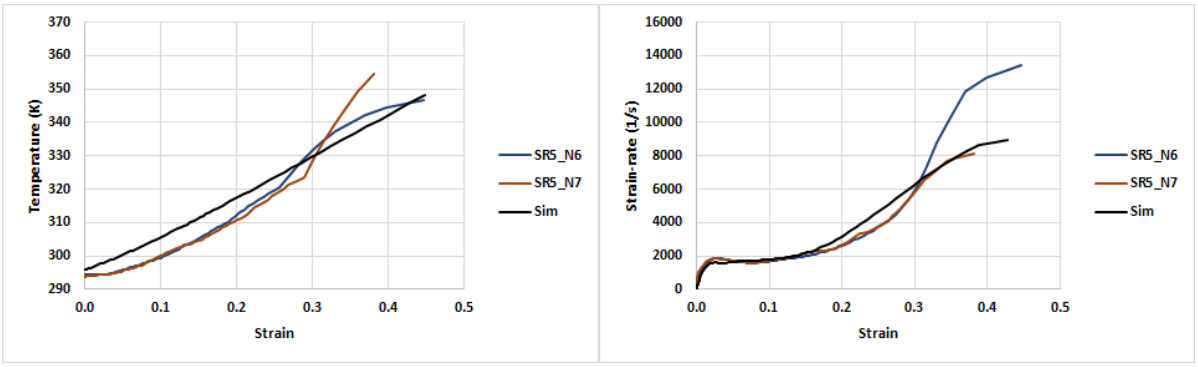

(a) (b)

Fig.5: Comparison between tests and thermal-structural coupled simulations for Al2024 at the SR5 rate; (a) temperature vs. strain, and (b) strain-rate vs. strain.

The additional rates, which were not covered by the physical tests and were added, are listed in Table 2. The thermal-structural coupled analyses at those rates generated the additional temperature-strain curves as shown in Fig.6. The selections of the analysis method and FE model at each rate are described in Table 2. The approximation method described in Section 4.2 estimated the calibrated effective TQC values at every rate as summarized in Table 2.

Name		Actual rate (1/sec)	Calibrated effective TQC (β)
R.0001	SR1	1.00E-04	0.00
R.001		1.00E-03	0.01
R.01		1.00E-02	0.02
R.1	SR2	1.00E-01	0.08
R.25		2.50E-01	0.15
R.5		5.00E-01	0.21
R1	SR3	1.00E+00	0.28
R2.5		2.50E+00	0.37
R5		5.00E+00	0.41
R10		1.00E+01	0.44
R100		1.00E+02	0.47
R500	SR4	5.00E+02	0.48
R2000	SR5	2.00E+03	0.49
R6000	SR6	6.00E+03	0.50

Table 2: Summary of additional simulations of Al2024.

The comparison of the temperature-strain curves between the thermal-structural coupled analysis and the structural-only analysis with the calibrated effective TQC table is shown in Fig.7. The shapes of temperature curves between two analyses are different, but the area under the curves at strains less than 0.3 are comparable. The strain value of 0.3 is the approximate erosion strain under tension of the Al2024 ***MAT_224** model.

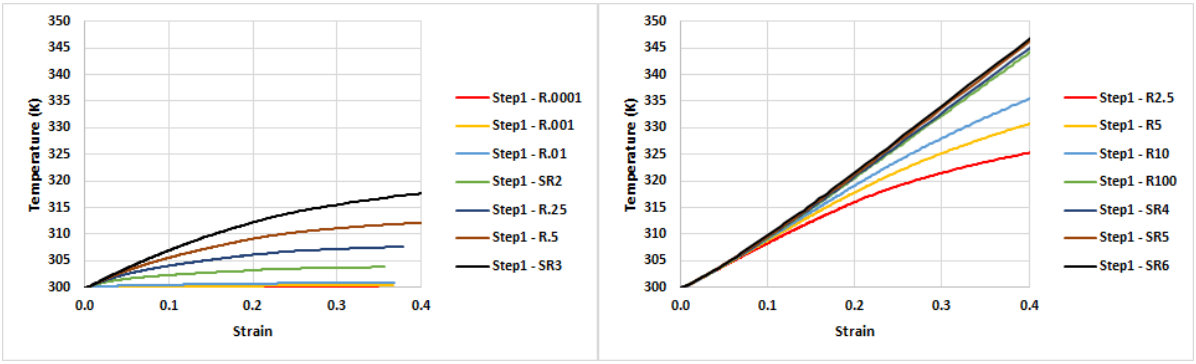

(a) (b)

Fig.6: Additional temperature vs. strain curves of Al2024; (a) at lower rates, and (b) at higher rates.

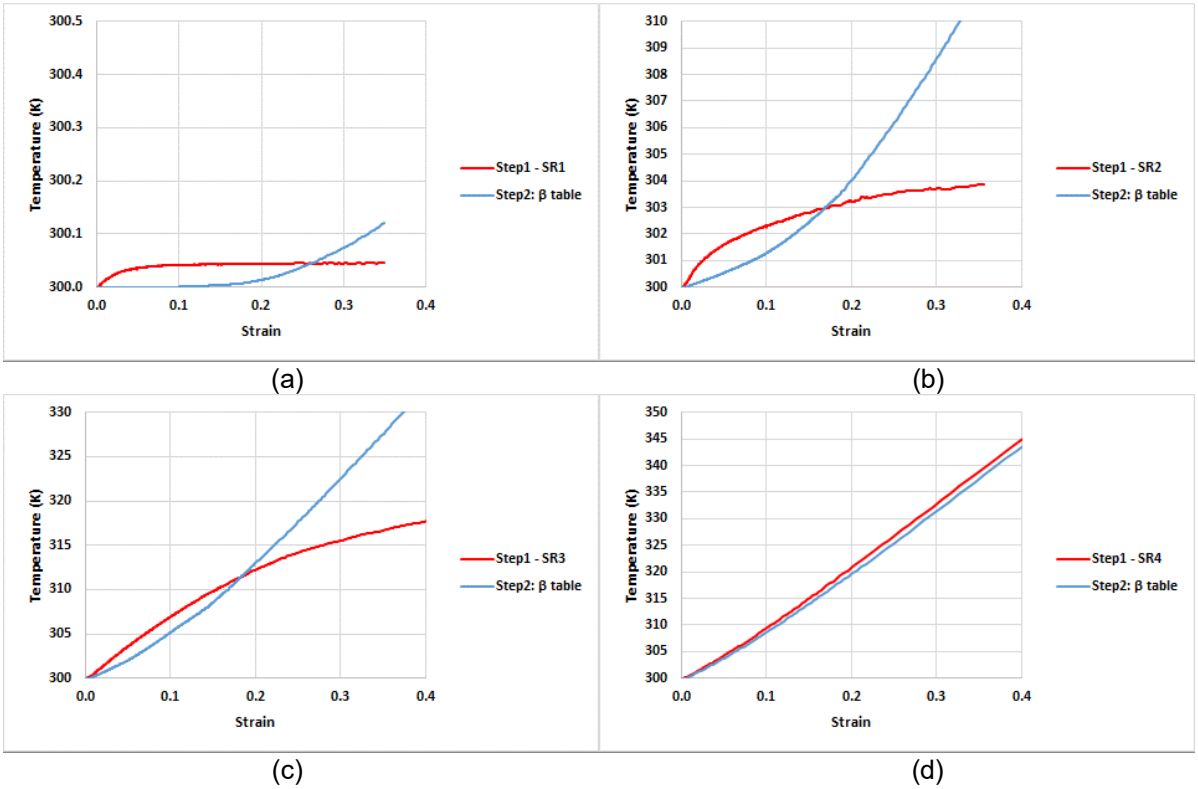

(a) (b)

(c) (d)

Fig.7: Comparison of temperature vs. strain curves between thermal-structural coupled analysis with the adjusted physical TQC and structural-only analysis with the calibrated effective TQC table on Al2024; (a) SR1 rate, (b) SR2 rate, (c) SR3 rate, and (d) SR4 rate.

7 Summary

Fig.8 summarizes all the different TQCs for Al2024. First, the green curves in Fig.8 show the referenced constant, physical TQC of the Al2024 *MAT_224 material model. The measured, effective TQC values, at different rates obtained from the physical tensile tests, are the red dots in Fig.8. The TQC table, the blue curves in Fig.8, is the calibrated, effective TQC curves obtained from simulations. It is observed that the measured TQC red dots correlate with the TQC table curves, with some deviation. The trends show that the TQC table curve could be fitted with a logistic function which is the yellow curves in Fig.8. The logistic function curves are very close to the TQC table curves in the low to mid-rate ranges, but they show some difference in the mid to high-rate ranges.

The original intention was to replace the constant TQC with the developed TQC tables. However, the adjusted physical TQC value of Al2024, which is the highest values in the TQC tables, are different from the referenced constant, physical TQC value. So, if the constant TQC is replaced with the TQC tables

directly, this change could be problematic for backward compatibility. Because the material dataset was developed based on the referenced physical TQC value, using the TQC table directly might cause simulation mismatches with ballistic test data. Therefore, at the highest strain rates in the Al2024 TQC table, the verified physical TQC values were modified to match the referenced physical TQC value. This final revision produces the modified TQC tables, the black dotted curves in Fig.8.

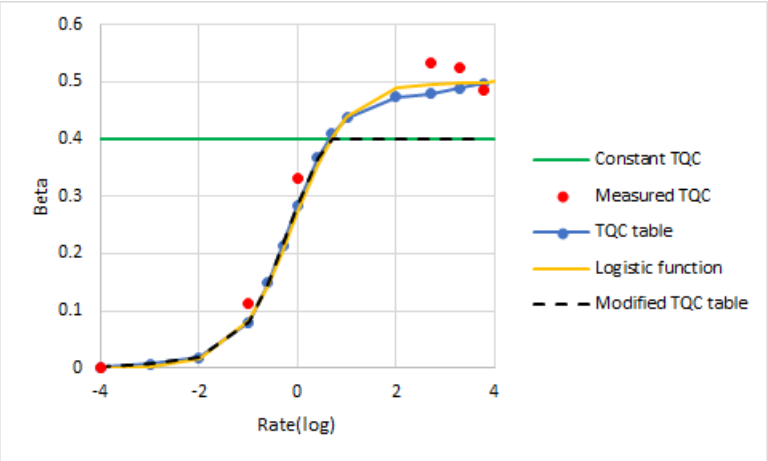

Fig.8: Summary of TQCs of Al2024

The use of an effective TQC table provides a way to overcome the absence of heat conduction in structural-only analysis using ***MAT_224**, so that *MAT_224 can be used for applications at low rates, as well as high rates. However, the inherent limitations of ***MAT_224** still remain. For instance, heat dissipation is dependent on material geometry and surrounding initial and boundary conditions, which means that effective TQC tables would theoretically need to be changed with different surrounding environments.

8 Acknowledgements

The authors would like to express our gratitude to Dr. Jarrod Smith, Dr. Jeremy Seidt, and Prof. Amos Gilat at Ohio State University, for sharing their insight and expertise along with the test data, photos, and videos generated during the tests. Their support greatly assisted with this research.

This research was conducted under FAA cooperative agreement 692M151840003 and sponsored by the Aircraft Catastrophic Failure Prevention Program.

9 Literature

[1] Emmerling, W., Altobelli, D., Carney, K., & Pereira, M. (2014). Development of a New Metal Material Model in LS-DYNA, Part 1: FAA, NASA, and Industry Collaboration Background. Technical Report, TC13-25-P1, Federal Aviation Administration, U.S. Department of Transportation. Retrieved from https://www.tc.faa.gov/its/worldpac/techrpt/tc13-25-p1.pdf

[2] Buyuk, M. (2014). Development of a New Metal Material Model in LS-DYNA, Part 2: Development of a Tabulated Thermo-Viscoplastic Material Model with Regularized Failure for Dynamic Ductile Failure Prediction of Structures under Impact Loading. Final Report, TC13-25-P2, Federal Aviation Administration, U.S. Department of Transportation. Retrieved from https://www.tc.faa.gov/its/worldpac/techrpt/tc13-25p2.pdf

[3] Park, C. K., Carney, K., Du Bois, P., Cordasco, D., & Kan, C. D. (2020). Aluminum 2024-T351 Input Parameters for ***MAT_224** in LS-DYNA. Final Report, TC19-41-P1, Federal Aviation Adminstration, U.S. Department of Transportation. Retrieved from https://www.tc.faa.gov/its/worldpac/techrpt/tc19-41-p1.pdf

[4] Seidt, J. D. (2014). Development of a New Metal Material Model in LS-DYNA, Part 3: Plastic Deformation and Ductile Fracture of 2024 Aluminum under Various Loading Conditions. Final Report, TC13-25-P3, Federal Aviation Administration, U.S. Department of Transportation. Retrieved from https://www.tc.faa.gov/its/worldpac/techrpt/tc13-25-p3.pdf

[5] Seidt, J. D., Park, C., Buyuk, M., Lowe, R. L., Wang, L., Carney, K. S., . . . Kan, C. (2022). An Experimental Investigation of the Influence of the State of Stress on the Ductile Fracture of 2024-T351 Aluminum. ASME Journal of Engineering Materials and Technology, 144, 041006-1.

[6] Seidt, J. D., Smith, J. L., Spulak, N., Lowe, R. L., & Gilat, A. (2022). Aluminum 2024-T351 Input Parameters for ***MAT_224** in LS-DYNA, Part 2: Additional tests to determine plastic heating and ductile fracture behavior under combined loading. Final Report, TC19-41-P2, Federal Aviation Administration, U.S. Department of Transportation. Retrieved from https://www.tc.faa.gov/its/worldpac/techrpt/tc19-41-p2.pdf

[7] Kelley, S., & Johnson, G. (2006). Statistical Testing of Aircraft Materials for Transport Airplane Rotor Burst Fragment Shielding. Final Report, AR06-9, Federal Aviation Administration, U.S. Department of Transportation. Retrieved from https://www.tc.faa.gov/its/worldpac/techrpt/AR06-9.pdf

[8] Pereira, M., Revilock, D., Lerch, B., & Ruggeri, C. (2013). Impact Testing of Aluminum 2024 and Titanium 6Al-4V for Material Model Development. Technical Memorandum, National Aeronautics and Space Administration. Retrieved from https://ntrs.nasa.gov/citations/20130013684

[9] Park, C. K., Queitzsch, G., Carney, K., Du Bois, P., Kan, C. D., Cordasco, D., & Emmerling, W. (2020). Aluminum 2024-T351 Input Parameters for ***MAT_224** in LS-DYNA, Part 3: Ballistic Impact Simulations of an Aluminum 2024 Panel Using ***MAT_224** in LS-DYNA Considering Oblique Incidence and Attitude Angles of a Rectangular Projectile. Final Report, TC19-41-P3, Federal Aviation Administration, U.S. Department of Transportation. Retrieved from https://www.tc.faa.gov/its/worldpac/techrpt/tc19-41-p3.pdf

[10] Park, C., Carney, K., Du Bois, P., Kan, C., & Cordasco, D. (2021). Aluminum 2024-T351 Input Parameters for ***MAT_224** in LS-DYNA, Part 4: Ballistic Impact Simulations of a Titanium 6Al-4V Generic Fan Blade Fragment on an Aluminum 2024 Panel Using ***MAT_224** in LS-DYNA. Final Report, TC19-41-P4, Federal Aviation Administration, U.S. Department of Transportation. Retrieved from https://www.tc.faa.gov/its/worldpac/techrpt/tc19-41-p4.pdf

[11] Ravichandran, G., Rosakis, A. J., Hodowany, J., & Rosakis, P. (2002). On the conversion of plastic work into heat during high-strain-rate deformation. AIP Conference Proceedings, 620, pp. 557-562.

[12] Smith, J. L. (2019). Full-Field Measurement of the Taylor-Quinney Coefficient in Tension Tests of Ti-6Al-4V, Aluminum 2024-T351, and Inconel 718 at Various Strain Rates. Technical Thesis, TCTT20-40, Federal Aviation Administration, U.S. Department of Transportation. Retrieved from https://www.tc.faa.gov/its/worldpac/techrpt/tctt20-40.pdf

[13] Park, C. K., Carney, K., Du Bois, P., & Kan, C. D. (2023, expected). Development of Effective Taylor-Quinney Coefficient Tables of *MAT_224 for Aluminum 2024-T351, Titanium 6Al-4V, and Inconel 718 Alloys. Final Report, In progress, Federal Aviation Adminstration, U.S. Department of Transportation.